Letter · Editors' Suggestion

Spatially indirect intervalley excitons in bilayer WSe_2

Zhiheng Huang,[1,2] Yanchong Zhao,[1,2] Tao Bo,[1,3] Yanbang Chu,[1,2] Jinpeng Tian,[1,2] Le Liu,[1,2] Yalong Yuan,[1,2] Fanfan Wu,[1,2] Jiaojiao Zhao,[1,2] Lede Xian,[3] Kenji Watanabe,[4] Takashi Taniguchi,[5] Rong Yang,[1,3,6] Dongxia Shi,[1,2,6] Luojun Du,[7,*] Zhipei Sun,[7,8] Sheng Meng,[1,2,3,†] Wei Yang,[1,2,6,‡] and Guangyu Zhang[1,2,3,6,§]

[1]*Beijing National Laboratory for Condensed Matter Physics; Key Laboratory for Nanoscale Physics and Devices, Institute of Physics, Chinese Academy of Sciences, Beijing 100190, China*

[2]*School of Physical Sciences, University of Chinese Academy of Sciences, Beijing 100190, China*

[3]*Songshan Lake Materials Laboratory, Dongguan, Guangdong Province 523808, China*

[4]*Research Center for Functional Materials, National Institute for Materials Science, 1-1 Namiki, Tsukuba 305-0044, Japan*

[5]*International Center for Materials Nanoarchitectonics, National Institute for Materials Science, 1-1 Namiki, Tsukuba 305-0044, Japan*

[6]*Beijing Key Laboratory for Nanomaterials and Nanodevices, Beijing 100190, China*

[7]*Department of Electronics and Nanoengineering, Aalto University, Tietotie 3, FI-02150 Espoo, Finland*

[8]*Quantum Technology Finland (QTF) Centre of Excellence, Department of Applied Physics, Aalto University, FI-00076 Aalto, Finland*

(Received 20 August 2021; revised 24 November 2021; accepted 15 December 2021; published 20 January 2022)

Spatially indirect excitons with displaced wave functions of electrons and holes play a pivotal role in a large portfolio of fascinating physical phenomena and emerging optoelectronic applications, such as valleytronics, exciton spin Hall effect, excitonic integrated circuit, and high-temperature superfluidity. Here, we uncover three types of spatially indirect excitons (including their phonon replicas) and their quantum-confined Stark effects in hexagonal boron nitride encapsulated bilayer WSe_2 by performing electric field-tunable photoluminescence measurements. Because of different out-of-plane electric dipole moments, the energy order between the three types of spatially indirect excitons can be switched by a vertical electric field. Remarkably, we demonstrate, assisted by first-principles calculations, that the observed spatially indirect excitons in bilayer WSe_2 are also momentum indirect, involving electrons and holes from Λ and K/Γ valleys in the Brillouin zone, respectively. This is in contrast to the previously reported spatially indirect excitons with electrons and holes localized in the same valley. Furthermore, we find that the spatially indirect intervalley excitons in bilayer WSe_2 can exhibit considerable, doping-sensitive circular polarization. The spatially indirect excitons with momentum-dark nature and highly tunable circular polarization may provide a firm basis for the understanding and engineering of technological applications in photonics and optoelectronics.

DOI: 10.1103/PhysRevB.105.L041409

Excitons, hydrogen-atom-like electron-hole pairs bound by their mutual Coulomb interaction, play an important role in a wide variety of intriguing optoelectronic properties of materials [1–4]. Depending on whether the wave functions of electrons and holes are spatially separated, excitons can be divided into two types: spatially direct and indirect excitons. Because of the separation of the electrons and holes, spatially indirect excitons have a much longer lifetime than spatially direct excitons and are predicted to exhibit a wide spectrum of emergent physical phenomena, including but not limit to quantum-confined Stark effect [5–7], Bose-Einstein condensation [8–14], strongly correlated excitonic insulator states [15–17], high-temperature superconductivity [18], valley physics [19–21], and dissipationless exciton transistors [22–24]. The recent emergence of two-dimensional transition metal dichalcogenides (TMDCs) and their van der Waals (vdW) heterostructures offers an unprecedented platform to realize spatially indirect excitons. Indeed, spatially indirect excitons have thus far been demonstrated in a wide variety of TMDC homo- and heterostructures [19], such as MoS_2/WS_2 [25–27], MoS_2/WSe_2 [28,29], $MoSe_2/WSe_2$ [20,22,30–33], and bilayer MoS_2 [7,34–39]. Specially, owing to the strongly reduced dielectric screening, spatially indirect excitons in homo-/heterobilayers of TMDCs possess substantial binding energies and show crucial advantages for applications, for example, superfluidity at high temperature [9].

To date, the studies of spatially indirect excitons have mainly focused on the momentum-bright species with electrons and holes localized in the same valley of the Brillouin zone (BZ) [7,19–25,29–42]. On the other hand, because of the existence of multiple electronic valleys, TMDC homo- and heterobilayers can also exhibit spatially indirect excitons with momentum-dark nature (that is, electrons and holes are from different valleys of the BZ) [6,28,43–45]. Since electrons and holes are further separated in momentum space, spatially indirect intervalley excitons, in principle, can possess a longer lifetime than spatially indirect but momentum-direct excitons and represent an advantageous scenario for numerous

*luojun.du@aalto.fi
†smeng@iphy.ac.cn
‡wei.yang@iphy.ac.cn
§gyzhang@iphy.ac.cn

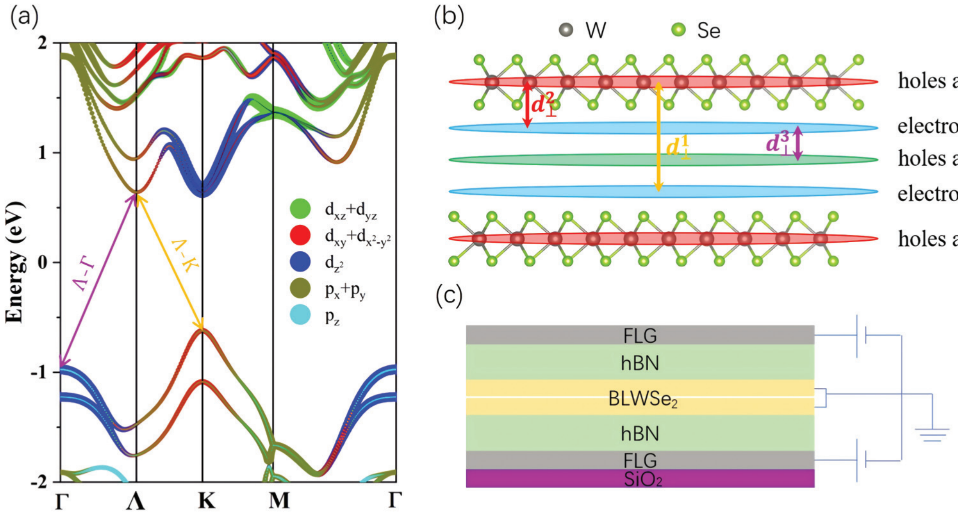

FIG. 1. (a) Orbital projected band structures of bilayer WSe_2. Symbol size is proportional to its population in corresponding state. (b) Schematic image of the equivalent positions of spin-up wave functions at K/K' (red ellipses), Λ/Λ' (blue ellipses), and Γ points (green ellipse) in real space. $d_\perp^{1-3}$ denote vertical distances between different wave functions. (c) Schematic of *h*-BN encapsulated bilayer WSe_2 device.

theoretical, experimental, and technological advances. However, in contrast to the well-studied spatially indirect excitons with momentum-bright features, experimental progress on spatially indirect intervalley excitons is still largely limited.

In this paper, we demonstrate three types of spatially indirect intervalley excitons (i.e., two Λ-*K* transitions, one Λ-Γ exciton, and their phonon replicas) and their quantum-confined Stark effects in hexagonal boron nitride (*h*-BN) encapsulated bilayer WSe_2 through the combination of electric field-dependent photoluminescence (PL) measurements and density functional theory (DFT) calculations. The energy order between the three types of spatially indirect intervalley excitons can be switched by an electric field, owing to their different electric dipole moments. Interestingly, these spatially indirect intervalley excitons in bilayer WSe_2 show considerable negative circular polarization that is highly tunable with electron doping. Our results not only provide a complete understanding of the puzzling multiplet emissions in WSe_2 bilayers but also present possibilities for valleytronics, high-temperature superfluidity, and advanced functionalities in photonics and optoelectronics.

Among various TMDCs, bilayer WSe_2 provides a promising platform for spatially indirect intervalley excitons. First, for bilayer WSe_2, the conduction band minimum is located at the Λ (Λ′) points of the BZ, while the critical points of the valence band are at K/K' and Γ, as shown in Fig. 1(a) [46–49]. Consequently, the lowest exciton transition in bilayer WSe_2 should be momentum-indirect Λ-*K* or Λ-Γ excitons, in marked contrast to the momentum-direct *K*-*K* transition in the monolayer case. Second, as the Bloch states at conduction band Λ and valence bands *K* and Γ have distinct orbital compositions [Fig. 1(a)], their wave functions show different interlayer hybridization and reside at different positions in real space [Fig. 1(b)] (Supplemental Material [50]) [47,51]. Therefore, momentum-indirect Λ-*K* and Λ-Γ excitons are also spatially indirect with finite out-of-plane electric dipole moments. Third, because of the substantial exciton-phonon coupling and the inevitable existence of defects [52–57], Λ-*K* and Λ-Γ transitions in bilayer WSe_2, in principle, can be activated by phonon/defect scattering and show strong PL responses. Although there have been some studies on spatially indirect intervalley excitons in bilayer WSe_2 [6,43,58–61], their underlying origin remains equivocal. In addition, previous researchers have reported only one type of Λ-*K* exciton [6,43], the other type of Λ-*K* transition and the Λ-Γ exciton have not been revealed.

We fabricated high-quality *h*-BN encapsulated bilayer WSe_2 devices by a vdW-mediated dry transfer method (see Supplemental Material [50] for more details). Few-layer graphene was used as both the bottom and top gate electrodes to further screen the charged impurities on SiO_2 substrates and improve the device quality [Fig. 1(c)]. Three *h*-BN encapsulated bilayer WSe_2 devices (labeled as D1, D2, and D3) were studied, showing similar behavior (see Supplemental Material [50] for more details). Unless otherwise specified, the data presented here are taken from device D1 in a high vacuum at 10 K, excited by 1.96 eV (633 nm) radiation. The dual-gated devices enabled us to independently tune the vertical electric field (E_z) and doping density (n_0) (Supplemental Material [50]).

Figure 2(a) shows the PL spectrum of bilayer WSe_2 without applying gate voltages. Apart from the momentum-direct *K*-*K* transitions at ~1.69 eV (X_0), seven lower energy peaks in the range of 1.50–1.65 eV (black dotted box), corresponding to the momentum-indirect transitions, can be clearly observed [6,59]. It is noteworthy that benefiting from the high quality of our samples, the number of momentum-indirect excitons revealed here is larger than that previously observed [6]. As we mentioned above, the momentum-indirect excitons in bilayer WSe_2 should also be spatially indirect. To confirm this, we performed electric-field-tunable PL measurements. Figure 2(b) depicts the color plot of PL spectra as a function of E_z. Obviously, all the momentum-indirect excitons are highly tunable with E_z, evidencing the quantum-confined Stark effects and their spatially indirect nature. Note that the emission energy of *K*-*K* transition X_0 remains unchanged

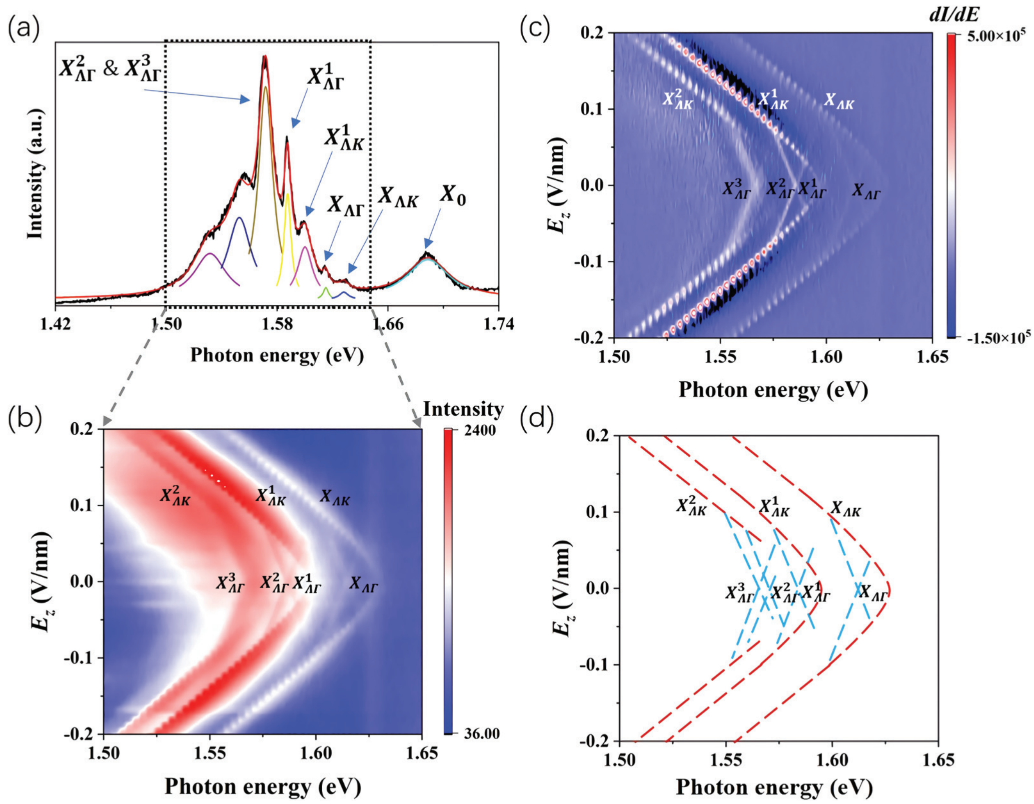

FIG. 2. (a) Photoluminescence (PL) spectrum of device D1 and its fitting under zero gate voltage. (b) Contour plot of the PL spectra as a function of photon energy (bottom axis) and E_z (left axis). n_0 remains unchanged. (c) First-order energy derivative of (b). Spatially indirect intervalley excitons are labeled as $X_{\Lambda K}$ ($X_{\Lambda\Gamma}$), $X^1_{\Lambda K}$ ($X^1_{\Lambda\Gamma}$) and $X^2_{\Lambda K}$ ($X^2_{\Lambda\Gamma}$ and $X^3_{\Lambda\Gamma}$) in sequence of decreasing emission energy. (d) Extracted emission energy as a function of E_z from (c) with red ($X_{\Lambda K}$ and $X^{1,2}_{\Lambda K}$) and blue ($X_{\Lambda\Gamma}$ and $X^{1-3}_{\Lambda\Gamma}$) dashed lines.

with E_z (Supplemental Material [50]). To better resolve the fine features, we plotted the first-order derivative of intensity ($\frac{\partial I}{\partial E}$) [Fig. 2(c)]. Figure 2(d) displays the energies of different spatially indirect intervalley emissions as a function of E_z, extracted from Fig. 2(c). The spatially indirect intervalley excitons in bilayer WSe_2, at first glance, can be divided into two types: one [blue dashed lines in Fig. 2(d)] with cross-shape features and the other [red dashed lines in Fig. 2(d)] with a conversion from nonlinear Stark shift at small $|E_z|$ to linear Stark shift at large $|E_z|$.

We tentatively assigned the former (latter) type of spatially indirect intervalley excitons as Λ-Γ (Λ-K) transitions. Note that, here, we use Λ-K transitions to denote all the possible transitions between electrons at Λ/Λ' and holes at K/K' and the same for Λ-Γ transitions. We extracted the vertical displacement of these excitons from Fig. 2(c) using $d_\perp = -\frac{\partial E}{e\cdot\partial E_Z}$, where E is the emission energy, and e is the elementary charge. Note that the sign of $d_\perp$ represents the direction of the electric dipole moment: positive (negative) means vertical upward (downward). For Λ-Γ transitions, the $d_\perp$ is nearly fixed at ± 1.40 Å [purple dots in Fig. 3(a)]. For Λ-K transitions, the $d_\perp$ is $\sim \pm 1.80$ Å at zero electric field; then it gradually increases with the electric field; and finally, it saturates at ± 4.50 Å [yellow dots in Fig. 3(b)].

To support our assignment, we then performed DFT calculations to derive the equivalent positions of spin-up/down wave functions at conduction band Λ and valence bands K and Γ. The equivalent position of a wave function is defined as $r_z = \int_{-\infty}^{+\infty} r|\varphi(r)|^2 dr$, where $|\varphi(r)|^2$ denotes the probability density of wave function $\varphi(r)$ at position r. The origin point (positive direction) is set as the midpoint between the two layers (vertical upward). For spin-up wave functions at conduction band Λ (Λ') and valence bands K (K') and Γ, the calculated equivalent positions at zero electric field are $r_z = -0.22t$ $(0.22t)$, $-0.48t\,(0.48t)$ and 0, respectively [Fig. 1(b)], where $t = 6.6$ Å is the interlayer distance of bilayer WSe_2. For spin-down wave functions, the equivalent positions can be obtained simply by time-reversal symmetry (Supplemental Material [50]). It is worth noting that the equivalent positions of $\pm 0.48t$ indicate the virtually suppressed interlayer hybridization and spin-layer locking for holes at K/K' [62–64].

For Λ-Γ transitions, there are two paths with equal transition probability [Fig. 3(c)]. One is from spin-up electrons at Λ to holes at Γ with $d_\perp = r_z(\Gamma) - r_z(\Lambda_\uparrow) = 1.45$ Å, and another is from spin-down electrons at Λ to holes at Γ with $d_\perp = r_z(\Gamma) - r_z(\Lambda_\downarrow) = -1.45$ Å. Here, we take transitions from Λ to Γ as an example; transitions from Λ' to Γ could give the same results (Supplemental Material [50]). Remarkably, $d_\perp$ obtained by first-principles calculations (± 1.45 Å) is in good agreement with the experiments (± 1.40 Å), confirming our assignment of Λ-Γ excitons [Fig. 3(a)].

For Λ-K transitions (here, we focus on spin-up holes at the K valley), there are four possible transition paths [Fig. 3(d)], depending on the spin and valley configuration of carriers. It is noteworthy that spatially indirect intervalley excitons

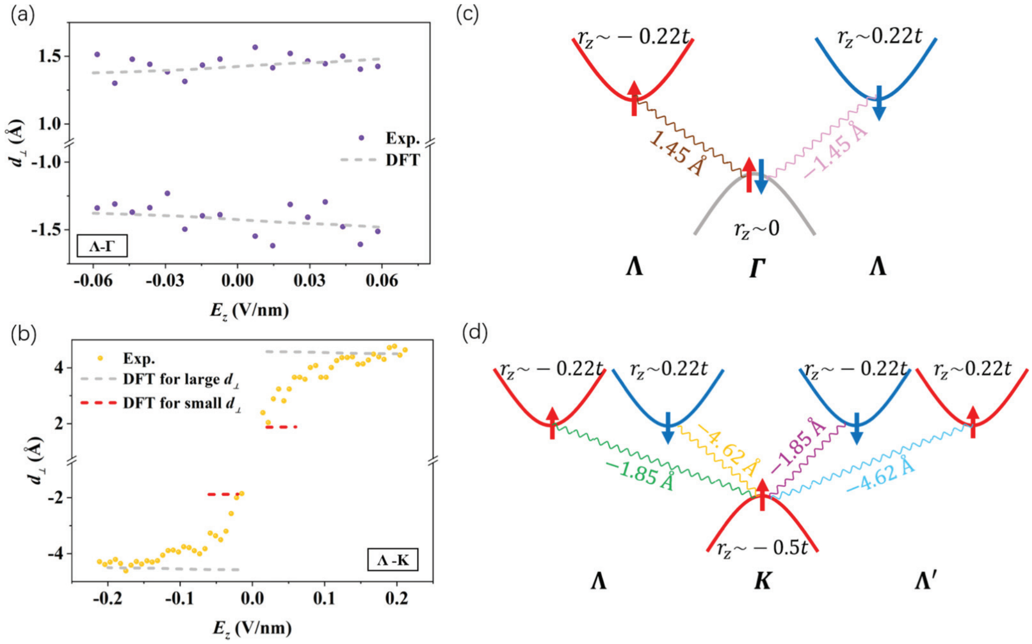

FIG. 3. (a) Experimental (purple dots) and calculated (dashed lines) vertical displacements of $X_{\Lambda\Gamma}$ as a function of E_z. (b) Experimental (yellow dots) and theoretically calculated (dashed lines) vertical displacements of $X_{\Lambda K}$ vs E_z. (c) and (d) Possible transition configurations of (c) $X_{\Lambda\Gamma}$ and (d) $X_{\Lambda K}$. $d_\perp$ of each configuration is denoted. Red (blue) curves represent spin-up (spin-down) bands. Valence Γ band is spin-degenerated. r_z denotes the equivalent position of wave function at zero electric field.

with spin-triplet configuration in bilayer WSe_2 may be bright because of the broken out-of-plane mirror symmetry [65]. Among the four possible transitions, two of them (i.e., transitions associated with spin-down electrons at Λ and spin-up electrons at Λ′) have a large $d_\perp(\sim -0.70t = -4.62$ Å), while the other two (i.e., transitions associated with spin-up electrons at Λ and spin-down electrons at Λ′) have a small $d_\perp(\sim -0.28t = -1.85$ Å) [Fig. 3(d)]. According to the spatial inversion symmetry, we know that, for spin-up holes at the K' valley, there are also four possible transitions but with opposite $d_\perp$: two of them with a large positive $d_\perp$ (∼4.62 Å) and the other two with a small positive $d_\perp$ (∼1.85 Å) (Supplemental Material [50]). For Λ-$K(K')$ transitions associated with spin-down holes, we can obtain similar results (Supplemental Material [50]). Again, a perfect agreement between theoretically calculated values and experimental results is obtained: $d_\perp = \pm 1.85$ and ± 4.62 Å obtained by DFT calculations match the experiments under zero electric field (±1.80 Å) and large electric fields (±4.50 Å) well [Fig. 3(b)]. Note that first-principles calculations show that $d_\perp$ change slightly with E_z [Figs. 3(a) and 3(b)]. For example, the large $d_\perp$ of Λ-K transition changes from ±4.62 Å at zero electric field to ±4.50 Å at $E_z = 0.2$ V/nm, which is more consistent with our experimental results [Fig. 3(b)]. In short, we reveal three types of spatially indirect intervalley excitons: two Λ-K transitions with different $d_\perp$ and one Λ-Γ exciton, providing a complete understanding of the multiplet emissions in bilayer WSe_2.

Remarkably, our results manifest three unique features for these spatially indirect intervalley excitons. First, from the comparison of experimental results and first-principles calculations, it can be known that Λ-K transition is dominated by the one with small $d_\perp$ at $E_z = 0$ and then gradually becomes dominated by the one with large $d_\perp$ as $|E_z|$ increases. Such an exotic characteristic of the Λ-K transition can be understood as follows. Since the wave functions of electrons and holes overlap more, Λ-K excitons with small $d_\perp$ possess larger binding energy than those with large $d_\perp$. As a result, Λ-K excitons with small $d_\perp$ have a lower energy and dominate the emission when $E_z = 0$ (Supplemental Material [50]). When E_z is applied, the larger Stark shift would lead the Λ-K transition with large $d_\perp$ to having a lower energy and thus more occupancy than that with small $d_\perp$. Consequently, the Λ-K transition with large $d_\perp$ would gain an increasing contribution and eventually dominate the emission under a strong electric field (e.g., $|E_z| > 0.1$ V/nm). Note that, under an intermediate electric field, the emission is a mixed state, contributed by both Λ-K transitions with large and small $d_\perp$. Second, for both Λ-K and Λ-Γ transitions, there are a series of replicas, labeled as $X_{\Lambda K}$ ($X_{\Lambda\Gamma}$), $X^1_{\Lambda K}$ ($X^1_{\Lambda\Gamma}$) and $X^2_{\Lambda K}$ ($X^2_{\Lambda\Gamma}$ and $X^3_{\Lambda\Gamma}$) in sequence of decreasing emission energy. For the two sets of highest-energy transitions (i.e., $X_{\Lambda K}$ and $X_{\Lambda\Gamma}$), the emission intensities are much darker than that of their replicas at lower energy (i.e., $X^{1,2}_{\Lambda K}$ and $X^{1,2,3}_{\Lambda\Gamma}$) [Fig. 2(b)], indicating that $X_{\Lambda K}/X_{\Lambda\Gamma}$ and $X^{1,2}_{\Lambda K}/X^{1,2,3}_{\Lambda\Gamma}$ have different origins. We tentatively attribute $X_{\Lambda K}$ ($X_{\Lambda\Gamma}$) and $X^{1,2}_{\Lambda K}$ ($X^{1,2,3}_{\Lambda\Gamma}$) to primary $\Lambda - K$ ($\Lambda - \Gamma$) transitions activated by defect scattering and their phonon replicas, respectively. Notably, the energy difference (∼42 meV) between the primary $X_{\Lambda K}$ ($X_{\Lambda\Gamma}$) and the phonon replica $X^2_{\Lambda K}$ ($X^3_{\Lambda\Gamma}$) that dominates the emission outstrips the single phonon energy in WSe_2 (∼37 meV) [56,66]. This indicates that phonon replicas come mainly from two-/multiphonon scattering, rather than one-phonon scattering. One plausible reason is that two-/multiphonon processes possess more scattering paths than one-phonon scattering. Third, $X_{\Lambda\Gamma}$ is ∼18 meV lower than $X_{\Lambda K}$ under zero electric field. This

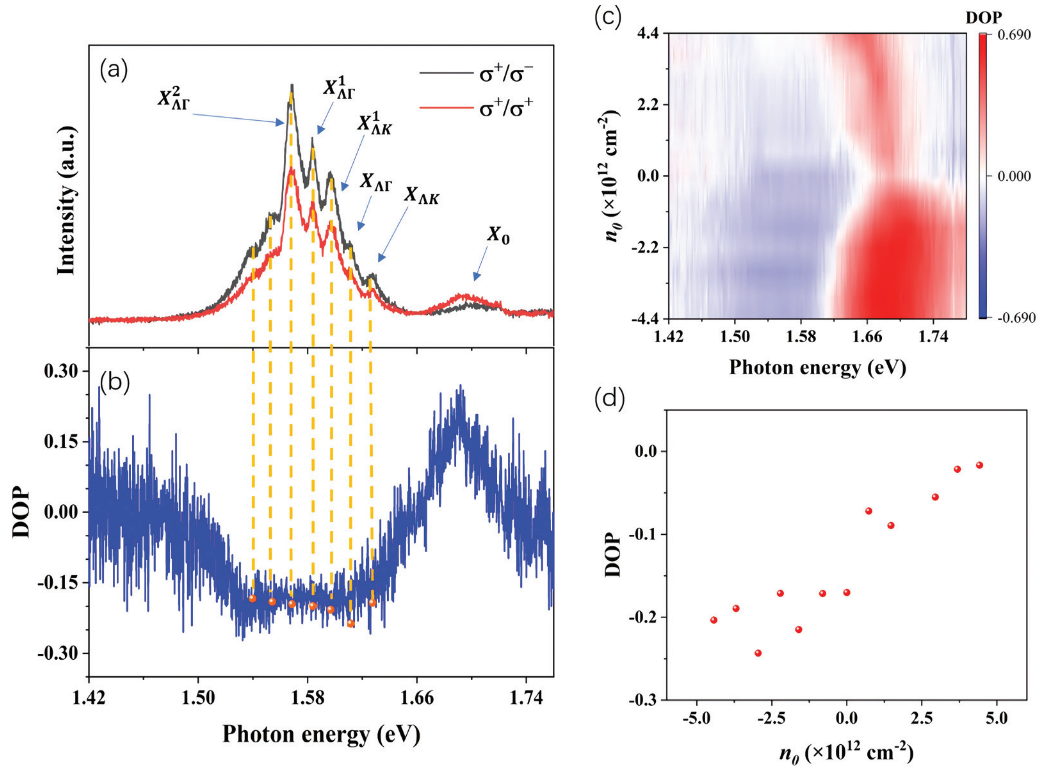

FIG. 4. (a) Photoluminescence (PL) spectra of device D2 under σ^+ (red line) and σ^- (black line) detections, excited by σ^+ light. (b) The degree of circular polarization (DOP) corresponding to (a) as a function of emission energy. DOPs calculated from the measured (blue line) and Lorentz-fitted intensities (orange dots) agree well with each other. (c) Contour plot of the DOP as a function of photon energy (bottom axis) and n_0 (left axis). E_z remains unchanged. (d) The DOP vs n_0, calculated from the integral intensity in the energy range from 1.45 to 1.60 eV. n_0 denotes the doping density induced by gate voltage.

seems a counterintuitive result because the valence Γ valley is located below the valence K valley [Fig. 1(a)] [6,49], which makes it natural to expect $X_{\Lambda\Gamma}$ to have higher emission energy than $X_{\Lambda K}$. In fact, the observed transition energy is determined by the difference between the electronic bandgap and the exciton binding energy rather than electronic bandgap only. Since the effective mass of holes at the Γ point ($\sim$1.01 m_e; m_e is the free electron mass) is much larger than that at the K point ($\sim$0.27 m_e) [46,60], $X_{\Lambda\Gamma}$ possesses a larger binding energy than $X_{\Lambda K}$, and thus, it can become the lower energy excitonic state.

Finally, we study the valley properties of spatially indirect intervalley excitons in bilayer WSe_2. Figure 4(a) shows the helicity-resolved PL spectra of device D2 for cocircularly (red) and cross-circularly polarized detections (black), excited by σ^+ radiation. We quantify the degree of circular polarization as $\mathrm{DOP} = \frac{I_{co}-I_{cross}}{I_{co}+I_{cross}}$, where I_{co} and I_{cross} denote the intensities detected under co- and cross-circularly polarized configurations, respectively. Figure 4(b) shows the DOP against the photon energy: the blue line is calculated directly from the measured intensities, while the orange dots present the DOP of spatially indirect intervalley excitons calculated from the fitting intensities. It is explicit that DOPs calculated from the measured and Lorentz-fitted intensities of each exciton peak agree well with each other. Thus, for simplicity, all the following DOPs are calculated directly with the measured intensities. Obviously, both Λ-K and Λ-Γ transitions evince considerable negative DOP (~ -0.2), whereas the momentum-direct K-K transition has a positive DOP. Furthermore, we find that the DOP of spatially indirect intervalley excitons in bilayer WSe_2 is highly tunable with doping density n_0 [Fig. 4(c)]. Figure 4(d) shows the DOP as a function of n_0, calculated with the integrated intensity from 1.45 to 1.60 eV. The DOP almost keeps constant for hole doping but gradually vanishes with increasing electron doping density. Such negative, highly tunable circular polarization of spatially indirect intervalley excitons may provide device paradigms to exploit the valley degree of freedom other than K (e.g., Λ and Γ). In-depth theoretical studies, however, are required to fully figure out the optical selection rules/intervalley coupling mechanisms/the role of phonons and further the highly tunable negative circular polarization of spatially indirect intervalley excitons in bilayer WSe_2 [67,68].

During the preparation of the manuscript, we became aware of a similar independent work by Altaiary *et al.* [69]. Both our work and the work by Altaiary *et al.* [69] clearly uncover the underlying origin of the multiplet emissions in bilayer WSe_2, resolving previous debates. Meanwhile, our work unveils more features. First, our results demonstrate that there are two Λ-K transitions with different $d_\perp$ and with increasing E_z, $X_{\Lambda K}$ gradually changes from the one with small $d_\perp$ to the one with large $d_\perp$, giving rise to the nonlinear Stark shift, while the work by Altaiary *et al.* [69] only reveals the Λ-K transition with large $d_\perp$. Second, we uncover the doping-tunable circular polarization of these spatially indirect intervalley excitons and their phonon replicas, providing a firm basis for photonics and optoelectronics.

In summary, we reveal three types of spatially indirect intervalley excitons (i.e., two Λ-K transitions, one Λ-Γ exciton, and their phonon replicas) and their giant Stark shift in bilayer WSe_2 encapsulated by *h*-BN. Owing to their different electric dipole moments, the energy order and dominant luminescence between the three types of spatially indirect intervalley excitons can be switched by a vertical electric field. Remarkably, these spatially indirect intervalley excitons in bilayer WSe_2 show considerable negative circular polarization that is highly tunable with doping density. Our results not only provide a deep understanding of the multiplet momentum-dark emissions in bilayer WSe_2 but also hold a promising future for dissipationless exciton transport, high-temperature superfluidity, and valley-functional optoelectronic devices with multiple quantum degrees of freedom.

All data needed to evaluate the conclusions in the paper are present in the paper and/or the Supplemental Material [50]. Additional data related to this paper may be requested from the authors.

We thank Yang Xu and Ting Wang in Institute of Physics, Chinese Academy of Sciences for useful discussion. This research was supported by the National Key Research and Development Program (Grants No. 2020YFA0309600 and No. 2018YFA0306900), the National Natural Science Foundation of China (Grants No. 61888102, No. 11834017, and No. 12074413), the Strategic Priority Research Program of CAS (Grants No. XDB30000000 and No. XDB33000000), the Key-Area Research and Development Program of Guangdong Province (Grant No. 2020B0101340001). L.D. gratefully acknowledges the financial support by Academy of Finland (Grant No. 333099). Z.S. acknowledges support from Academy of Finland (Grants No. 314810, No. 333982, No. 336144, and No. 336818), Academy of Finland Flagship Programme (Grant No. 320167, PREIN), the European Union's Horizon 2020 research and innovation program (Grants No. 820423, S2QUIP; and No. 965124, FEMTOCHIP), the EU H2020-MSCARISE-872049 (IPN-Bio), and the European Research Council (Grant No. 834742). K.W. and T.T. acknowledge support from the Elemental Strategy Initiative conducted by the Ministry of Education, Culture, Sports, Science and Technology, Japan, Grant No. JPMXP0112101001, Japan Society for the Promotion of Science KAKENHI Grant No. JP20H00354, and the CREST (JPMJCR15F3), JST.

Z.H., Y.Z., and T.B. contributed equally to this paper. G.Z. and W.Y. supervised this paper; Z.H. and Y.Z. conceived the project and designed the experiments; Z.H. fabricated the devices and carried out the optical measurements; T.B. and S.M. conducted the first-principles calculations; K.W. and T.T. contributed high-quality *h*-BN crystals; Z.H., Y.Z., L.D., and W.Y. analyzed the data; Z.H., Y.Z., L.D., W.Y., and G.Z. cowrote the manuscript. All authors discussed the results and commented on the paper.

The authors declare that they have no competing interests.

[1] G. Wang, A. Chernikov, M. M. Glazov, T. F. Heinz, X. Marie, T. Amand, and B. Urbaszek, *Colloquium*: Excitons in atomically thin transition metal dichalcogenides, Rev. Mod. Phys. **90**, 021001 (2018).

[2] A. Tartakovskii, Excitons in 2D heterostructures, Nat. Rev. Phys. **2**, 8 (2020).

[3] G. D. Scholes and G. Rumbles, Excitons in nanoscale systems, Nat. Mater. **5**, 683 (2006).

[4] C. Jin, E. Y. Ma, O. Karni, E. C. Regan, F. Wang, and T. F. Heinz, Ultrafast dynamics in van der Waals heterostructures, Nat. Nanotechnol. **13**, 994 (2018).

[5] K. F. Mak and J. Shan, Opportunities and challenges of interlayer exciton control and manipulation, Nat. Nanotechnol. **13**, 974 (2018).

[6] Z. F. Wang, Y. H. Chiu, K. Honz, K. F. Mak, and J. Shan, Electrical tuning of interlayer exciton gases in WSe_2 bilayers, Nano Lett. **18**, 137 (2018).

[7] N. Leisgang, S. Shree, I. Paradisanos, L. Sponfeldner, C. Robert, D. Lagarde, A. Balocchi, K. Watanabe, T. Taniguchi, X. Marie *et al.*, Giant Stark splitting of an exciton in bilayer MoS_2, Nat. Nanotechnol. **15**, 901 (2020).

[8] J. P. Eisenstein and A. H. Macdonald, Bose-Einstein condensation of excitons in bilayer electron systems, Nature (London) **432**, 691 (2004).

[9] Z. F. Wang, D. A. Rhodes, K. Watanabe, T. Taniguchi, J. C. Hone, J. Shan, and K. F. Mak, Evidence of high-temperature exciton condensation in two-dimensional atomic double layers, Nature (London) **574**, 76 (2019).

[10] J. I. A. Li, T. Taniguchi, K. Watanabe, J. Hone, and C. R. Dean, Excitonic superfluid phase in double bilayer graphene, Nat. Phys. **13**, 751 (2017).

[11] X. Liu, K. Watanabe, T. Taniguchi, B. I. Halperin, and P. Kim, Quantum Hall drag of exciton condensate in graphene, Nat. Phys. **13**, 746 (2017).

[12] M. M. Fogler, L. V. Butov, and K. S. Novoselov, High-temperature superfluidity with indirect excitons in van der Waals heterostructures, Nat. Commun. **5**, 4555 (2014).

[13] Q. Shi, E.-M. Shih, D. A. Rhodes, B. Kim, K. Barmak, K. Watanabe, T. Taniguchi, Z. Papi´c, D. A. Abanin, J. Hone *et al.*, Bilayer WSe_2 as a natural platform for interlayer exciton condensates in the strong coupling limit, arXiv:2108.10477 (2021).

[14] C. Lagoin and F. Dubin, Key role of the moiré potential for the quasicondensation of interlayer excitons in van der Waals heterostructures, Phys. Rev. B **103**, L041406 (2021).

[15] L. Ma, P. X. Nguyen, Z. Wang, Y. Zeng, K. Watanabe, T. Taniguchi, A. H. MacDonald, K. F. Mak, and J. Shan, Strongly correlated excitonic insulator in atomic double layers, Nature (London) **598**, 585 (2021).

[16] J. Gu, L. Ma, S. Liu, K. Watanabe, T. Taniguchi, J. C. Hone, J. Shan, and K. F. Mak, Dipolar excitonic insulator in a moire lattice, arXiv:2108.06588 (2021).

[17] Z. Zhang, E. C. Regan, D. Wang, W. Zhao, S. Wang, M. Sayyad, K. Yumigeta, K. Watanabe, T. Taniguchi, S. Tongay *et al.*, Correlated interlayer exciton insulator in double layers of monolayer WSe_2 and moiré WS_2/WSe_2, arXiv:2108.07131 (2021).

[18] Y. E. Lozovik and V. I. Yudson, A new mechanism for superconductivity: pairing between spatially separated electrons and holes, Zh. Eksp. Teor. Fiz **71**, 738 (1976).

[19] P. Rivera, H. Y. Yu, K. L. Seyler, N. P. Wilson, W. Yao, and X. D. Xu, Interlayer valley excitons in heterobilayers of transition metal dichalcogenides, Nat. Nanotechnol. **13**, 1004 (2018).

[20] P. Rivera, K. L. Seyler, H. Yu, J. R. Schaibley, J. Yan, D. G. Mandrus, W. Yao, and X. Xu, Valley-polarized exciton dynamics in a 2D semiconductor heterostructure, Science **351**, 688 (2016).

[21] Z. Huang, Y. Liu, K. Dini, Q. Tan, Z. Liu, H. Fang, J. Liu, T. Liew, and W. Gao, Robust room temperature valley Hall effect of interlayer excitons, Nano Lett. **20**, 1345 (2020).

[22] L. A. Jauregui, A. Y. Joe, K. Pistunova, D. S. Wild, A. A. High, Y. Zhou, G. Scuri, K. De Greve, A. Sushko, C. H. Yu *et al.*, Electrical control of interlayer exciton dynamics in atomically thin heterostructures, Science **366**, 870 (2019).

[23] D. Unuchek, A. Ciarrocchi, A. Avsar, K. Watanabe, T. Taniguchi, and A. Kis, Room-temperature electrical control of exciton flux in a van der Waals heterostructure, Nature (London) **560**, 340 (2018).

[24] D. Unuchek, A. Ciarrocchi, A. Avsar, Z. Sun, K. Watanabe, T. Taniguchi, and A. Kis, Valley-polarized exciton currents in a van der Waals heterostructure, Nat. Nanotechnol. **14**, 1104 (2019).

[25] H. Heo, J. H. Sung, S. Cha, B.-G. Jang, J.-Y. Kim, G. Jin, D. Lee, J.-H. Ahn, M.-J. Lee, J. H. Shim *et al.*, Interlayer orientation-dependent light absorption and emission in monolayer semiconductor stacks, Nat. Commun. **6**, 7372 (2015).

[26] M. Okada, A. Kutana, Y. Kureishi, Y. Kobayashi, Y. Saito, T. Saito, K. Watanabe, T. Taniguchi, S. Gupta, Y. Miyata *et al.*, Direct and indirect interlayer excitons in a van der Waals heterostructure of hBN/WS_2/MoS_2/hBN, ACS Nano **12**, 2498 (2018).

[27] Y. Zhao, T. Bo, L. Du, J. Tian, X. Li, K. Watanabe, T. Taniguchi, R. Yang, D. Shi, S. Meng *et al.*, Thermally induced band hybridization in bilayer-bilayer MoS_2/WS_2 heterostructure, Chin. Phys. B **30**, 057801 (2021).

[28] J. Kunstmann, F. Mooshammer, P. Nagler, A. Chaves, F. Stein, N. Paradiso, G. Plechinger, C. Strunk, C. Schüller, G. Seifert *et al.*, Momentum-space indirect interlayer excitons in transition-metal dichalcogenide van der Waals heterostructures, Nat. Phys. **14**, 801 (2018).

[29] O. Karni, E. Barré, S. C. Lau, R. Gillen, E. Y. Ma, B. Kim, K. Watanabe, T. Taniguchi, J. Maultzsch, K. Barmak *et al.*, Infrared Interlayer Exciton Emission in MoS_2/WSe_2 Heterostructures, Phys. Rev. Lett. **123**, 247402 (2019).

[30] P. Rivera, J. R. Schaibley, A. M. Jones, J. S. Ross, S. F. Wu, G. Aivazian, P. Klement, K. Seyler, G. Clark, N. J. Ghimire *et al.*, Observation of long-lived interlayer excitons in monolayer $MoSe_2-WSe_2$ heterostructures, Nat. Commun. **6**, 6242 (2015).

[31] E. R. Liu, E. Barre, J. van Baren, M. Wilson, T. Taniguchi, K. Watanabe, Y. T. Cui, N. M. Gabor, T. F. Heinz, Y. C. Chang *et al.*, Signatures of moiré trions in WSe_2/$MoSe_2$ heterobilayers, Nature (London) **594**, 46 (2021).

[32] P. Nagler, M. V. Ballottin, A. A. Mitioglu, F. Mooshammer, N. Paradiso, C. Strunk, R. Huber, A. Chernikov, P. C. M. Christianen, C. Schüller *et al.*, Giant magnetic splitting inducing near-unity valley polarization in van der Waals heterostructures, Nat. Commun. **8**, 1551 (2017).

[33] M. Brotons-Gisbert, K. Baek, A. Campbell, K. Watanabe, T. Taniguchi, and B. D. Gerardot, Moiré-Trapped Interlayer Trions in a Charge-Tunable WSe_2/$MoSe_2$ Heterobilayer, Phys. Rev. X **11**, 031033 (2021).

[34] I. C. Gerber, E. Courtade, S. Shree, C. Robert, T. Taniguchi, K. Watanabe, A. Balocchi, P. Renucci, D. Lagarde, X. Marie *et al.*, Interlayer excitons in bilayer MoS_2 with strong oscillator strength up to room temperature, Phys. Rev. B **99**, 035443 (2019).

[35] I. Niehues, A. Blob, T. Stiehm, S. M. de Vasconcellos, and R. Bratschitsch, Interlayer excitons in bilayer MoS_2 under uniaxial tensile strain, Nanoscale **11**, 12788 (2019).

[36] A. Arora, T. Deilmann, P. Marauhn, M. Drüppel, R. Schneider, M. R. Molas, D. Vaclavkova, S. Michaelis de Vasconcellos, M. Rohlfing, M. Potemski *et al.*, Valley-contrasting optics of interlayer excitons in Mo- and W-based bulk transition metal dichalcogenides, Nanoscale **10**, 15571 (2018).

[37] E. Lorchat, M. Selig, F. Katsch, K. Yumigeta, S. Tongay, A. Knorr, C. Schneider, and S. Höfling, Excitons in Bilayer MoS_2 Displaying a Colossal Electric Field Splitting and Tunable Magnetic Response, Phys. Rev. Lett. **126**, 037401 (2021).

[38] Y. Zhao, L. Du, S. Yang, J. Tian, X. Li, C. Shen, J. Tang, Y. Chu, K. Watanabe, T. Taniguchi *et al.*, Optically and magnetically addressable valley pseudospin of interlayer excitons in bilayer MoS_2, arXiv:2106.00351 (2021).

[39] N. Peimyoo, T. Deilmann, F. Withers, J. Escolar, D. Nutting, T. Taniguchi, K. Watanabe, A. Taghizadeh, M. F. Craciun, K. S. Thygesen *et al.*, Electrical tuning of optically active interlayer excitons in bilayer MoS_2, Nat. Nanotechnol. **16**, 888 (2021).

[40] A. Arora, M. Drüppel, R. Schmidt, T. Deilmann, R. Schneider, M. R. Molas, P. Marauhn, S. Michaelis de Vasconcellos, M. Potemski, M. Rohlfing *et al.*, Interlayer excitons in a bulk van der Waals semiconductor, Nat. Commun. **8**, 639 (2017).

[41] C. Jin, E. C. Regan, D. Wang, M. I. B. Utama, C.-S. Yang, J. Cain, Y. Qin, Y. Shen, Z. Zheng, K. Watanabe *et al.*, Identification of spin, valley and moiré quasi-angular momentum of interlayer excitons, Nat. Phys. **15**, 1140 (2019).

[42] J. Choi, M. Florian, A. Steinhoff, D. Erben, K. Tran, D. S. Kim, L. Sun, J. Quan, R. Claassen, S. Majumder *et al.*, Twist Angle-Dependent Interlayer Exciton Lifetimes in van der Waals Heterostructures, Phys. Rev. Lett. **126**, 047401 (2021).

[43] G. Scuri, T. I. Andersen, Y. Zhou, D. S. Wild, J. Sung, R. J. Gelly, D. Bérubé, H. Hoseok, L. Shao, A. Y. Joe *et al.*, Electrically Tunable Valley Dynamics in Twisted WSe_2/WSe_2 Bilayers, Phys. Rev. Lett. **124**, 217403 (2020).

[44] L. Yuan, B. Zheng, J. Kunstmann, T. Brumme, A. B. Kuc, C. Ma, S. Deng, D. Blach, A. Pan, and L. Huang, Twist-angle-dependent interlayer exciton diffusion in WS_2-WSe_2 heterobilayers, Nat. Mater. **19**, 617 (2020).

[45] J. Sung, Y. Zhou, G. Scuri, V. Zólyomi, T. I. Andersen, H. Yoo, D. S. Wild, A. Y. Joe, R. J. Gelly, H. Heo *et al.*, Broken mirror symmetry in excitonic response of reconstructed domains in twisted $MoSe_2$/$MoSe_2$ bilayers, Nat. Nanotechnol. **15**, 750 (2020).

[46] A. Kormanyos, G. Burkard, M. Gmitra, J. Fabian, V. Zolyomi, and N. D. Drummond, and V. Fal'ko, $\mathbf{k}\cdot\mathbf{p}$ theory for two-dimensional transition metal dichalcogenide semiconductors, 2D Mater. **2**, 022001 (2015).

[47] G. B. Liu, D. Xiao, Y. G. Yao, X. D. Xu, and W. Yao, Electronic structures and theoretical modelling of two-dimensional group-VIB transition metal dichalcogenides, Chem. Soc. Rev. **44**, 2643 (2015).
[48] N. R. Wilson, P. V. Nguyen, K. Seyler, P. Rivera, A. J. Marsden, Z. P. L. Laker, G. C. Constantinescu, V. Kandyba, A. Barinov, N. D. M. Hine *et al.*, Determination of band offsets, hybridization, and exciton binding in 2D semiconductor heterostructures, Sci. Adv. **3**, e1601832 (2017).
[49] P. V. Nguyen, N. C. Teutsch, N. P. Wilson, J. Kahn, X. Xia, A. J. Graham, V. Kandyba, A. Giampietri, A. Barinov, G. C. Constantinescu *et al.*, Visualizing electrostatic gating effects in two-dimensional heterostructures, Nature (London) **572**, 220 (2019).
[50] See Supplemental Material at http://link.aps.org/supplemental/10.1103/PhysRevB.105.L041409 for details on device fabrication, electric field-dependent PL spectra and DOP, results of device D2 and D3, equivalent positions of spin-down wave functions, possible transition configurations of Λ'-Γ transitions, Λ-K$'$ transitions associated with spin-up holes and Λ-K/Λ-K$'$ transitions associated with spin-down holes, and first-principles calculations, which includes Refs. [70–76].
[51] L. J. Du, T. T. Zhang, M. Z. Liao, G. B. Liu, S. P. Wang, R. He, Z. P. Ye, H. Yu, R. Yang, D. X. Shi *et al.*, Temperature-driven evolution of critical points, interlayer coupling, and layer polarization in bilayer MoS_2, Phys. Rev. B **97**, 165410 (2018).
[52] M. H. He, P. Rivera, D. V. Tuan, N. P. Wilson, M. Yang, T. Taniguchi, K. Watanabe, J. Q. Yan, D. G. Mandrus, H. Y. Yu *et al.*, Valley phonons and exciton complexes in a monolayer semiconductor, Nat. Commun. **11**, 618 (2020).
[53] E. Liu, J. van Baren, C.-T. Liang, T. Taniguchi, K. Watanabe, N. M. Gabor, Y.-C. Chang, and C. H. Lui, Multipath Optical Recombination of Intervalley Dark Excitons and Trions in Monolayer WSe_2, Phys. Rev. Lett. **124**, 196802 (2020).
[54] E. Liu, J. van Baren, T. Taniguchi, K. Watanabe, Y.-C. Chang, and C. H. Lui, Valley-selective chiral phonon replicas of dark excitons and trions in monolayer WSe_2, Phys. Rev. Research **1**, 032007(R) (2019).
[55] Z. P. Li, T. M. Wang, C. H. Jin, Z. G. Lu, Z. Lian, Y. Z. Meng, M. Blei, S. Y. Gao, T. Taniguchi, K. Watanabe *et al.*, Emerging photoluminescence from the dark-exciton phonon replica in monolayer WSe_2, Nat. Commun. **10**, 2469 (2019).
[56] L. J. Du, M. Z. Liao, J. Tang, Q. Zhang, H. Yu, R. Yang, K. Watanabe, T. Taniguchi, D. X. Shi, Q. M. Zhang *et al.*, Strongly enhanced exciton-phonon coupling in two-dimensional WSe_2, Phys. Rev. B **97**, 235145 (2018).
[57] P. Rivera, M. He, B. Kim, S. Liu, C. Rubio-Verdú, H. Moon, L. Mennel, D. A. Rhodes, H. Yu, T. Taniguchi *et al.*, Intrinsic donor-bound excitons in ultraclean monolayer semiconductors, Nat. Commun. **12**, 871 (2021).
[58] G. Wang, X. Marie, L. Bouet, M. Vidal, A. Balocchi, T. Amand, D. Lagarde, and B. Urbaszek, Exciton dynamics in WSe_2 bilayers, Appl. Phys. Lett. **105**, 182105 (2014).
[59] J. Lindlau, M. Selig, A. Neumann, L. Colombier, J. Forste, V. Funk, M. Forg, J. Kim, G. Berghauser, T. Taniguchi *et al.*, The role of momentum-dark excitons in the elementary optical response of bilayer WSe_2, Nat. Commun. **9**, 2586 (2018).
[60] W. J. Zhao, R. M. Ribeiro, M. L. Toh, A. Carvalho, C. Kloc, A. H. C. Neto, and G. Eda, Origin of indirect optical transitions in few-layer MoS_2, WS_2, and WSe_2, Nano Lett. **13**, 5627 (2013).
[61] P. Chen, C. Cheng, C. Shen, J. Zhang, S. Wu, X. Lu, S. Wang, L. Du, K. Watanabe, T. Taniguchi *et al.*, Band evolution of two-dimensional transition metal dichalcogenides under electric fields, Appl. Phys. Lett. **115**, 083104 (2019).
[62] A. M. Jones, H. Y. Yu, J. S. Ross, P. Klement, N. J. Ghimire, J. Q. Yan, D. G. Mandrus, W. Yao, and X. D. Xu, Spin-layer locking effects in optical orientation of exciton spin in bilayer WSe_2, Nat. Phys. **10**, 130 (2014).
[63] Z. R. Gong, G. B. Liu, H. Y. Yu, D. Xiao, X. D. Cui, X. D. Xu, and W. Yao, Magnetoelectric effects and valley-controlled spin quantum gates in transition metal dichalcogenide bilayers, Nat. Commun. **4**, 2053 (2013).
[64] L. Du, M. Liao, G.-B. Liu, Q. Wang, R. Yang, D. Shi, Y. Yao, and G. Zhang, Strongly distinct electrical response between circular and valley polarization in bilayer transition metal dichalcogenides, Phys. Rev. B **99**, 195415 (2019).
[65] H. Yu, G.-B. Liu, and W. Yao, Brightened spin-triplet interlayer excitons and optical selection rules in van der Waals heterobilayers, 2D Mater. **5**, 035021 (2018).
[66] X. Luo, Y. Zhao, J. Zhang, M. Toh, C. Kloc, Q. Xiong, and S. Y. Quek, Effects of lower symmetry and dimensionality on Raman spectra in two-dimensional WSe_2, Phys. Rev. B **88**, 195313 (2013).
[67] M. Selig, F. Katsch, R. Schmidt, S. Michaelis de Vasconcellos, R. Bratschitsch, E. Malic, and A. Knorr, Ultrafast dynamics in monolayer transition metal dichalcogenides: Interplay of dark excitons, phonons, and intervalley exchange, Phys. Rev. Research **1**, 022007(R) (2019).
[68] G. Berghauser, I. Bernal-Villamil, R. Schmidt, R. Schneider, I. Niehues, P. Erhart, S. Michaelis de Vasconcellos, R. Bratschitsch, A. Knorr, and E. Malic, Inverted valley polarization in optically excited transition metal dichalcogenides, Nat. Commun. **9**, 971 (2018).
[69] M. M. Altaiary, E. Liu, C.-T. Liang, F.-C. Hsiao, B. J. van, T. Taniguchi, K. Watanabe, N. M. Gabor, Y.-C. Chang, and C. H. Lui, Electric-field-tunable intervalley excitons and phonon replicas in bilayer WSe_2, arXiv:2101.11161 (2021).
[70] F. Pizzocchero, L. Gammelgaard, B. S. Jessen, J. M. Caridad, L. Wang, J. Hone, P. Boggild, and T. J. Booth, The hot pick-up technique for batch assembly of van der Waals heterostructures, Nat. Commun. **7**, 11894 (2016).
[71] L. Wang, I. Meric, P. Y. Huang, Q. Gao, Y. Gao, H. Tran, T. Taniguchi, K. Watanabe, L. M. Campos, D. A. Muller *et al.*, One-dimensional electrical contact to a two-dimensional material, Science **342**, 614 (2013).
[72] K. Kim, S. Larentis, B. Fallahazad, K. Lee, J. M. Xue, D. C. Dillen, C. M. Corbet, and E. Tutuc, Band alignment in WSe_2-graphene heterostructures, ACS Nano **9**, 4527 (2015).
[73] J. P. Perdew, K. Burke, and M. Ernzerhof, Generalized Gradient Approximation Made Simple, Phys. Rev. Lett. **77**, 3865 (1996).
[74] G. Kresse and J. Furthmuller, Efficient iterative schemes for ab initio total-energy calculations using a plane-wave basis set, Phys. Rev. B **54**, 11169 (1996).
[75] P. E. Blochl, Projector augmented-wave method, Phys. Rev. B **50**, 17953 (1994).
[76] J. Klimes, D. R. Bowler, and A. Michaelides, Van der Waals density functionals applied to solids, Phys. Rev. B **83**, 195131 (2011).